energies

MDPI

Article

Thermo-Oxidative Aging Effect on Charge Transport in Polypropylene/Ultra-High Molecular Weight Polyethylene Nanocomposites

Phichet Ketsamee *, Orestis Vryonis, Alun Vaughan and Thomas Andritsch

The Tony Davies High Voltage Laboratory, University of Southampton, Southampton SO17 1BJ, UK; o.vryonis@soton.ac.uk (O.V.); asv@ecs.soton.ac.uk (A.V.); t.andritsch@soton.ac.uk (T.A.)
* Correspondence: pk1r18@soton.ac.uk

Abstract: This study investigates the impact of magnesium oxide (MgO) nanoparticles on the thermo-oxidative aging behavior of blends of polypropylene (PP) and ultra-high molecular weight polyethylene (UHMWPE). The samples, both unfilled and filled with MgO, were aged at 120 °C for varying durations of up to 672 h. The observed structural changes are not monotonic; recrystallization leads to the increased crystallinity and melting temperature of UHMWPE until 336 h. Beyond this, the consumption of the antioxidant leads to chain scission which, in turn, results in decreased crystallinity. The presence of carbonyl groups indicates chemical changes and, as such, the carbonyl index is used as an indicator of aging, with subsequent changes to charge transport. During thermal aging, the interaction between PP and UHMWPE chains at interfaces is enhanced, leading to improved compatibility and the emergence of a new single crystallization peak in PP/UHMWPE blends. Although MgO does not show evidence of elevating the crystallization temperature, implying the absence of enhanced nucleation, it acts as a compatibilizer, improving interfacial interaction compared with the unfilled blend counterparts. MgO hinders the breakage of molecular structures and impedes the diffusion of oxygen. This, in turn, results in nanocomposites filled with MgO having reduced their charge accumulation and conductivity, thus delaying the aging process compared to PP/UHMWPE blends without nanofiller.

Keywords: carbonyl index; chain scission; charge transport; magnesium oxide; polypropylene; recrystallization; thermo-oxidative aging; ultra-high molecular weight polyethylene

Citation: Ketsamee, P.; Vryonis, O.; Vaughan, A.; Andritsch, T. Thermo-Oxidative Aging Effect on Charge Transport in Polypropylene/Ultra-High Molecular Weight Polyethylene Nanocomposites. *Energies* **2023**, *16*, 6670. https://doi.org/10.3390/en16186670

Academic Editors: Nick Tucker and Nikola Chalashkanov

Received: 23 August 2023
Revised: 11 September 2023
Accepted: 15 September 2023
Published: 18 September 2023

1. Introduction

Thermo-oxidative aging is a process of the degradation of polymer-based materials caused by a combination of elevated temperatures and exposure to oxygen as a function of time. The accelerated thermo-oxidative aging of insulation materials, such as cross-linked polyethylene (XLPE), has been extensively studied. Kim et al. [1] demonstrated that aging XLPE at 120 °C led to the formation of carbonyl groups, altering the material's melting behavior and indicating chain scission and oxidation reactions, resulting in decreased resistivity. The thermo-oxidative process involves the breaking of carbon and hydrogen bonds, depending on the concentration of antioxidants in XLPE, leading to the production of hydrogen peroxide, which further reacts to produce carbonyl groups [2]. The presence of these carbonyl groups then increases charge accumulation, leading to increased polarization at low frequency, and consequently, higher dielectric losses at a low frequency is associated with significant cable aging [3].

Polypropylene (PP) allows for a potentially higher operating temperature than XLPE, up to 160 °C. The high melting point potentially eliminates the need for crosslinking agents, thus prevents by-product formation and eliminates the requirement for lengthy degassing procedures [4]. Additionally, PP being a thermoplastic means it is more easily recyclable at the end of its service life compared to XLPE [5]. PP is also a non-polar polymer with

good hydrophobicity, making it suitable for cable insulation that maintains consistent performance under various humidity conditions, particularly for submarine cables [6]. In terms of its dielectric properties, PP possesses a high breakdown strength, low dielectric permittivity, and high DC volume resistivity [7].

However, using PP without any additives in HV cables is not feasible due to its brittleness resulting from its high glass transition temperature [8]. Additionally, PP has significantly lower thermal conductivity compared to PE-based compounds [9], limiting the potential benefits of its higher melting point. In a previous study [10], the addition of 50 weight percentage (wt.%) of ultra-high molecular weight polyethylene (UHMWPE) powder into PP matrix increased thermal conductivity from 0.21 W/m·K to 0.31 W/m·K, primarily attributed to the long molecular chains of UHMWPE. The incompatibility between PP and UHMWPE, as well as the weak bonding strength of their interfaces resulted in enhanced elasticity. However, this weak boundary was the main factor contributing to the reduction in breakdown strength.

The addition of magnesium oxide (MgO) nanoparticles of up to 3 wt.% in PP/UHMWPE blends was found to further improve the dielectric, thermal, and mechanical performances [10]. PP/UHMWPE/MgO nanocomposites resulted in an increase in thermal conductivity of up to 0.33 W/m·K. Due to the lack of a connected network at these low MgO levels, the enhanced thermal conductivity of nanocomposites is limited. The addition of MgO nanoparticles acts as a compatibilizer between two immiscible polymer blends, enhancing the interaction at the interface and further improving elasticity and elongation at break when compared to PP/UHMWPE blends. Moreover, this enhanced interfacial interaction results in an increase in breakdown strength.

While the aforementioned work [10] showed that PP/UHMWPE/MgO nanocomposites have some potential as insulation materials for HV power cables, their long-term performance requires further investigation. The influence of nanoparticles on the thermo-oxidative process and their impact on dielectric performance were studied in XLPE samples with and without MgO nanoparticles that underwent thermal aging at 135 °C for 720 h [11]. The calculated carbonyl index (CI) for the nanocomposite was 1.04, whereas it reached 1.68 for neat XLPE. This resulted in a 38% decrease in breakdown strength for neat XLPE, while the decrease in the nanocomposite was 20% compared to its unaged samples. In addition, low-density polyethylene (LDPE)-based nanocomposites containing 1 wt.% of silica (SiO_2), zinc oxide (ZnO), and MgO nanoparticles were subjected to aging at 90 °C for 1848 h, as studied in [12,13]. Among these nanocomposites, LDPE/MgO displayed the best performance.

This study aimed to explore the structural changes and chemical characteristics that may impact the dielectric performance of PP/UHMWPE blends with and without the inclusion of MgO nanoparticles. PP/UHMWPE blends and PP/UHMWPE/MgO nanocomposites are prepared using the solvent blending method. This approach simplifies achieving uniformly dispersed nanoparticles within a polymer matrix when using a suitable solvent [14,15]. Furthermore, preparing polymer-based materials with UHMWPE using high-temperature melt-mixing methods could result in the molecular entanglement or breakage of the long molecular chains of UHMWPE due to high shear stresses [16]. These would result in a lesser increase in thermal conductivity when compared to solvent blending [17,18]. The prepared samples are subjected to thermal aging at 120 °C for different periods ranging from 0 to 672 h. Structural characteristics are analyzed using differential scanning calorimetry (DSC) and X-ray diffraction (XRD). Chemical modifications are investigated using Fourier transform infrared (FTIR) spectroscopy. The dielectric performance of the samples is evaluated by measuring the space charge dynamics and DC conductivity.

2. Materials, Sample Preparation, and Aging Procedure

2.1. Materials

The samples used in this study were produced from PP pellets (427,861) with a melting temperature of approximately 160–165 °C and an average molecular weight of

approximately 340,000 g/mol, as well as UHMWPE powder (429,015) with an average molecular weight ranging from 3×10^6 to 6×10^6 g/mol. Both systems were obtained from Sigma Aldrich (Dorset, UK). MgO nano powder, with a mean particle size of 10–30 nm, was purchased from SkySpring Nanomaterial, Inc. (Houston, TX, USA). The silane coupling agent, 3-aminopropyl triethoxy (EA), was obtained from Aladdin Industrial Inc. (Shanghai, China).

2.2. Sample Preparations and Aging Procedure

The technique for the surface functionalization of MgO with EA using an anhydrous method was established in [19]. The selection of ethoxy-modified MgO nanoparticles at 1 wt.% is based on previous works [19,20]. Under both dry and humid conditions, better dielectric properties were observed in EA-modified systems, when compared to TiO_2 and MgO nanoparticles modified with 3-trimethoxysilyl propyl methacrylate and 3-aminopropyl trimethoxy silanes in a PP matrix.

PP/UHMWPE blends and PP/UHMWPE/MgO nanocomposites were prepared using a solution blending method. In the blends, a ratio of 50 wt.% of PP and UHMWPE was mixed, while in the nanocomposites, 1 wt.% of MgO replaced an equal weight of UHMWPE in the PP/UHMWPE mixture. Surface-modified MgO nano powder was initially sonicated in 5 mg/mL of xylene for 30 min to break up agglomerations before adding it to a PP/xylene mixture. The UHMWPE powder was then mixed with 245 mg/mL of xylene in the PP/MgO solvent after 1 min of continuous stirring. The mixture was then stirred for an additional minute before being poured into 90 mL of methanol. The resulting precipitated solid was first dried for 24 h in a fume cupboard and then fully dried for 72 h in a vacuum oven at 80 °C. The final, dried product was pressed at 180 °C to produce plates with a thickness of 200 ± 10 μm and a diameter of 50 mm for most tests (for measurements of DC conductivity, 70 mm diameter specimens were used instead). Finally, the films were quenched in distilled water at room temperature (~20 °C), and then stored in a desiccator until further use.

The samples, prepared as described earlier, underwent thermal aging in a fan oven (Memmert UF 30) at 120 °C for various durations from 0 to 672 h. Throughout the thermal aging, both surfaces of each sample were exposed to the air, to ensure uniform oxidative reactions across the sample thickness. After the completion of the aging process, the samples were allowed to naturally cool down to room temperature. Subsequently, the aged films were stored in a vacuum desiccator to minimize the influence of ambient humidity on any subsequent measurements. The composition of each sample and its corresponding aging conditions are summarized in Table 1.

Table 1. Composition of each sample and its aging conditions.

Materials	Compositions (wt.%)			Temperature (°C)	Aging Time (Hours)
	PP	UHMWPE	MgO		
PP/UHMWPE	50	50	-	120	Unaged 168 336 504 672
PP/UHMWPE/MgO	50	49	1		

The uniformity of such an aging approach is evinced by Tantipattarakul et al., who aged blends of LDPE/high-density polyethylene (HDPE) with a thickness of 200 μm at 120 °C for 720 h [21]. The authors used confocal Raman mapping to measure the carbonyl index across the sample thickness and found negligible variation in Raman scattering throughout the sample thickness.

3. Characterization Techniques

Alterations in the crystalline structure as a consequence of thermal aging were investigated via XRD with a Bruker Power X-ray D2 Phaser. Diffraction patterns were recorded over a 2θ range of 10°–80°, with an incremental step size of 0.0202°, employing a Cu Kα X-ray source with a wavelength of 1.54184 Å, and operating at 30 kV and 10 mA.

The melting and crystallization behavior of the PP and UHMWPE phases was characterized using a Mettler Toledo DSC-820 differential scanning calorimeter. Samples weighing ~5 mg were placed in aluminum containers and were then heated from 20 °C to 200 °C, held at 200 °C for 5 min, before finally being cooled back to 20 °C. Both the heating and cooling processes were carried out at a rate of 10 °C/min in a nitrogen atmosphere.

FTIR spectra in attenuated total reflection (ATR) mode were acquired using a Thermo Scientific Nicolet iS5 FT-IR Spectrometer equipped with iD7 AR diamond crystal plates. The spectral data were collected over a range of 525–4000 cm^{-1} and each spectrum was generated by averaging 16 scans at a resolution of 4 cm^{-1}.

Space charge dynamics data were acquired using a pulsed electro-acoustic (PEA) system following the IEC/TS 62,758 standard [22]. A pulse signal with an amplitude of 600 V, a pulse width of 5 ns, at a frequency of 400 Hz was applied. To enhance the acoustic signal, silicone oil was applied between the samples and the electrodes. The samples were initially calibrated at a +5 kV/mm electric field at room temperature and then tested for 1 h under an applied electric field of +40 kV/mm (poling). Immediately afterwards, each sample was short-circuited, and data were acquired for an additional hour (de-poling). All collected space charge data were analyzed using LabVIEW.

DC conductivity measurement was performed following the ASTM D257-14 standard [23]. The samples were placed between two gold-coated electrodes, and the measuring electrode had a 30 mm diameter guarding. The conduction current was monitored every 1 s for a duration of 1 h using a Keithley 486 picometer. The measurements were carried out at room temperature during a period of 3600 s, using an applied field of +40 kV/mm, and the data were collected and analyzed using LabVIEW.

4. Results

4.1. Thermal and Crystal Evaluations

As no significant changes in cross-section morphology were observed in scanning electron microscopy (SEM) between unaged and thermo-oxidatively aged samples, the analysis of the morphology was omitted from this paper. This is consistent with the SEM results presented in [24,25], which suggest that subjecting PP to thermal aging at 120 °C has no impact on the structure of PP. Figure 1 shows the XRD patterns acquired from PP/UHMWPE and PP/UHMWPE/MgO samples after thermal aging at 120 °C for durations ranging from 0 to 672 h. The XRD diffractogram of neat PP displays distinct peaks at 2θ = 14.1°, 17°, 18.6°, 21.3°, 21.8°, 25.6°, and 28.7°, which match with the (110), (040), (130), (111), (131)/(041), (060), and (220) crystal planes of the α-crystal (monoclinic) structure [26,27]. The diffractogram of UHMWPE shows peaks at 2θ values of 21.6°, 24°, and 36.3°, which correspond to the (110), (200), and (020) crystal planes of orthorhombic PE crystals [28]. The presence of face-centered cubic structured MgO nanoparticles is indicated by the peaks located at 36.9° (111), 42.9° (200), and 62.3° (220) [29]. In the unaged PP/UHMWPE blends and PP/UHMWPE/MgO nanocomposites, the presence of UHMWPE and MgO does not affect the crystal forms of PP. Notably, there are no distinct peaks corresponding to the β(300) crystal form (2θ = 16°) in the PP phase, which is different from other reports [30,31], where UHMWPE was observed to induce the β(300) crystal form in PP. However, in both types of samples, the (110) reflection in UHMWPE is combined with the (111) and (131)/(041) reflections of PP.

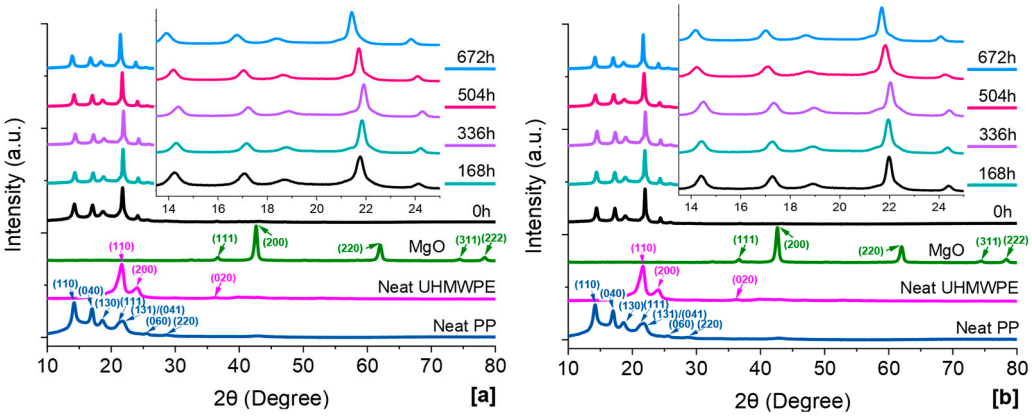

Figure 1. XRD diffractogram of (**a**) PP/UHMWPE and (**b**) PP/UHMWPE/MgO systems, thermally aged at 120 °C from 0 to 672 h.

Due to thermal aging, the crystalline structures in both the PP/UHMWPE and PP/UHMWPE/MgO samples shift towards lower diffraction angles, specifically beyond 336 h. The relationship between the interplanar spacing (d-spacing) between atoms and the diffraction angle can be expressed by Bragg's law ($2d \sin\theta = n\lambda$), where λ represents the wavelength of XRD [32]. It can be inferred that the interplanar spacing is inversely related to the angle of diffraction. Thus, based on the XRD spectra in Figure 1, it is evident that aging for more than 336 h leads to an increase in interplanar spacing. This increase suggests an expansion of the lattice in the polymers. Comparing PP/UHMWPE blends to PP/UHMWPE/MgO nanocomposites demonstrates that the XRD peaks exhibited a similar trend. This observation aligns with the findings in [11], where XRD shifted to lower diffraction angles, which were observed in XLPE and XLPE/MgO nanocomposites. The expansion of lattices is attributed to the increase in defects and damage to the crystalline structure caused by oxidation reactions [2,33].

Figure 2 shows the first scan of the melting (T_m) and crystallization (T_c) temperatures of PP/UHMWPE blends and PP/UHMWPE/MgO nanocomposites aged for different durations (0–672 h) at 120 °C, as recorded via DSC. In the unaged materials, the melting behavior is described by two distinct peaks around 130 °C and 162 °C, representing the UHMWPE and PP phases, respectively. As thermal aging progressed, the T_m in the UHMWPE phase of the blends sharply increased within 336 h, after which the T_m increase became less pronounced with further thermal aging (as depicted in Figure 3). Similarly, the nanocomposites displayed comparable behavior, albeit with a lesser change in the T_m of the UHMWPE phase compared to the blends. After 336 h of aging, the T_m of PP/UHMWPE blends exhibited an increase from 130.2 ± 0.2 °C to 137.2 ± 0.2 °C, while the nanocomposites experienced a rise from 130.6 ± 0.2 °C to 136.1 ± 0.3 °C. Conversely, no changes were observed in the PP phase of both PP/UHMWPE and PP/UHMWPE/MgO during the thermal aging process. As for the second scan of all aged samples, no difference in T_m was observed in each PP or UHMWPE component compared to the unaged samples. As such, these results were omitted from this paper.

With respect to T_c, as depicted in Figure 2b,d, the nanocomposites exhibit no alteration in their crystallization behavior after thermal aging, with a consistent single crystallization peak, maximum at 118 °C. This implies that there is no evidence of MgO elevating the crystallization temperature, suggesting the absence of enhanced nucleation. On the other hand, the blends exhibited a transition from a bimodal crystallization behavior in the unaged samples to a single crystallization peak as the aging time increased. The crystallization peak in both components shifted towards an intermediate point and remained at 118 °C, similarly to the behavior observed in the nanocomposites.

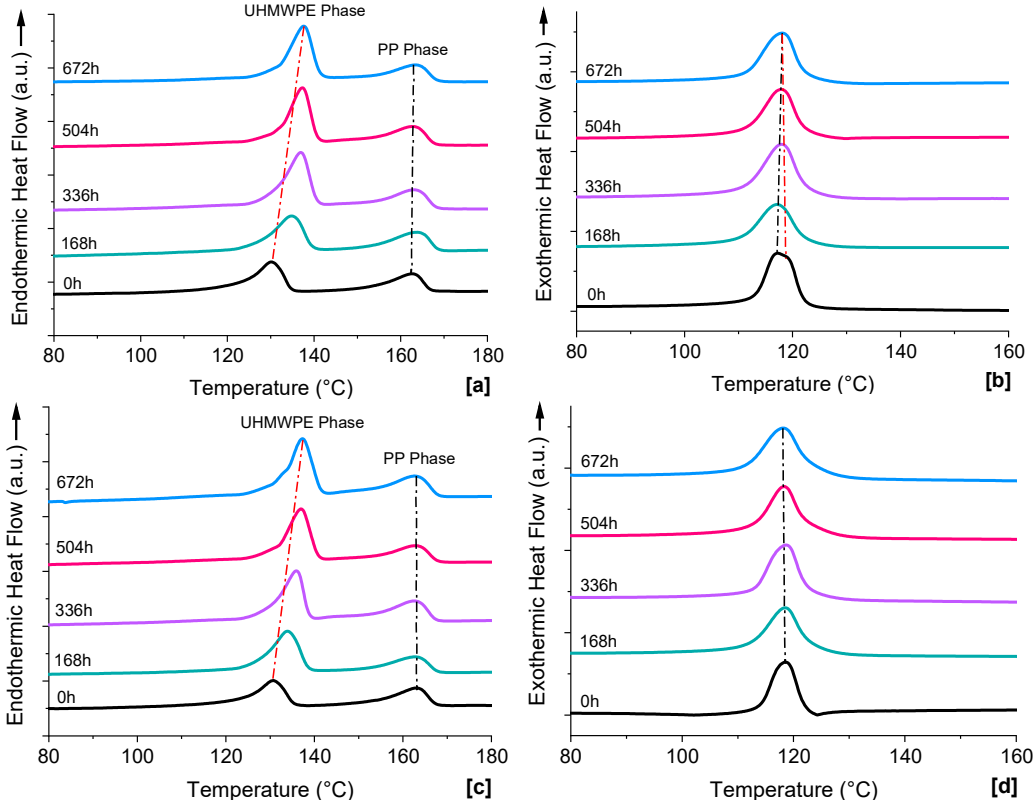

Figure 2. Melting temperatures of (**a**) PP/UHMWPE and (**c**) PP/UHMWPE/MgO, as well as crystallization temperatures of (**b**) PP/UHMWPE and (**d**) PP/UHMWPE/MgO aged at 120 °C.

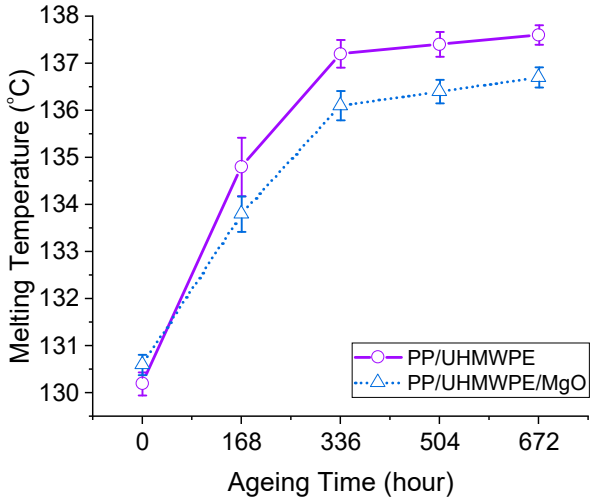

Figure 3. Changes in melting temperature of UHMWPE phases in PP/UHMWPE and PP/UHMWPE/MgO at 120 °C thermal aging.

Previous work demonstrated that the of PP and UHMWPE is 113 °C and 119 °C, respectively [10]. Increasing the UHMWPE content up to 50 wt.% raised the T_c of PP to 117 °C [10]. The increase in T_c of PP with higher UHMWPE content in unaged immiscible PP/UHMWPE blends is attributed to heterogeneous surface nucleation at the interfaces, which is influenced by the total number of interfaces and the melt viscosity in the blend system [31,34,35]. In terms of the new single crystallization of PP/UHMWPE blends seen after thermal aging, this can be attributed to the annealing effect, leading to the recrystallization of polymer chains. Since only the T_m of UHMWPE changes in Figure 2, this indicates that the molecular chains of UHMWPE can undergo increased molecular

mobility and recrystallization. As time progresses, the long UHMWPE chains diffuse across phase boundaries, impeding the chain relaxation of PP and promoting nucleation sites for the formation of a new crystalline phase at the PP/UHMWPE interfaces [31,36].

Figure 4 presents a quantitative comparison of the impact of the aging time on overall crystallinity, as revealed by XRD (χ_{XRD}) and DSC (χ_{DSC}). χ_{XRD} was calculated by dividing the total area of the crystalline peaks by the area of all peaks [37], while χ_{DSC} was obtained using Equations (1) and (2) [38–40]:

$$\chi_{c,PP}(\%) = \frac{\Delta H_{m,PP}}{(1-w)\Delta H^0_{m,PP}} \times 100\% \quad (1)$$

$$\chi_{c,UHMWPE}(\%) = \frac{\Delta H_{m,UHMWPE}}{w\Delta H^0_{m,UHMWPE}} \times 100\% \quad (2)$$

where $\chi_{c,PP}$ and $\chi_{c,UHMWPE}$ denote the crystallinities of the PP and UHMWPE phases, respectively. The melting enthalpies of 100% crystalline PP $\left(\Delta H^0_{m,\,PP}\right)$ and UHMWPE $\left(\Delta H^0_{m,UHMWPE}\right)$ are 167 J/g [38,40] and 293 J/g [39], respectively. $\Delta H_{m,PP}$ and $\Delta H_{m,UHMWPE}$ are the melting enthalpies of PP and UHMWPE, respectively. w is the weight fraction of UHMWPE in the blends.

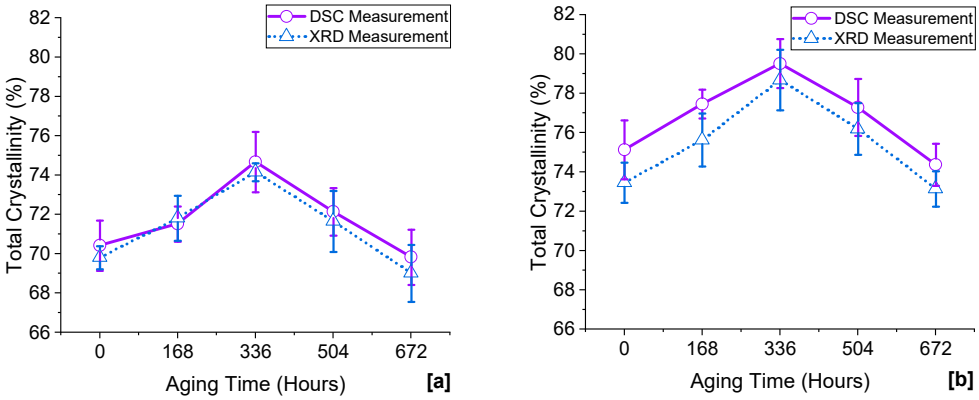

Figure 4. The overall crystallinity measured in XRD and DSC techniques for (**a**) PP/UHMWPE and (**b**) PP/UHMWPE/MgO.

Both techniques show a similar trend in χ_{XRD} and χ_{DSC} values: the impact of aging, especially within the first 336 h, appears to be influenced by recrystallization conditions, resulting in increased crystallinity. However, as the aging period increases, the rate of degradation increases following antioxidant consumption, which is associated with a drastic chain scission and a deteriorated crystal structure [2,21,41], as indicated by the drop in crystallinity.

As observed in the XRD measurement (Figure 1), the overlapping peaks of (111) and (130)/(041) of the PP phases and (110) of the UHMWPE phase do not provide a direct determination of the changes in crystallinity for each component. The crystallinity of each polymer was, therefore, considered by DSC alone, as shown in Figure 5. Only the crystallinity in the UHMWPE phase changes, which aligns with the general trend in the overall crystallinity shown in Figure 4. This implies that applying thermal aging at 120 °C only affects the UHMWPE chains into two distinct ways: recrystallization or chain scission. Conversely, the molecular chain of the PP phase remains unaffected. This finding corresponds to the results presented in references [24,25,42], which indicates that the thermal aging of PP, PP blended with an elastomer, and PP nanocomposites at temperatures lower than 130 °C for durations of up to 672 h had no impact on the PP structure. However, when aging PP and its composites at temperatures closer to the T_m of PP, i.e., 140 °C [24,43],

the recrystallization of PP structures resulted in an increase of 3–4 °C in T_m and a 6% increase in crystallinity.

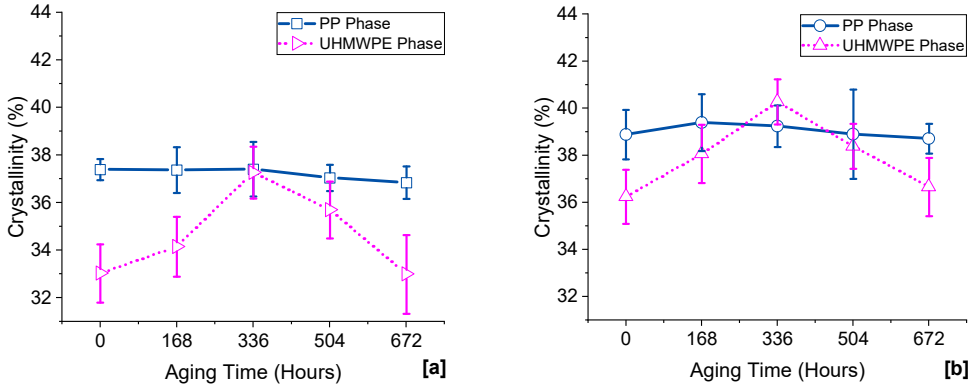

Figure 5. Crystallinity in PP and UHMWPE phases measured in DSC technique of (**a**) PP/UHMWPE and (**b**) PP/UHMWPE/MgO.

In addition, the effects of thermo-aging reactions on the molar mass changes in PP and UHMWPE were observed using gel permeation chromatography (GPC), as reported elsewhere [44,45]. PP aged between 95 °C and 125 °C exhibited a 5% drop in molar mass after 1500 h of aging [44]. A significant drop in molar mass occurred when PP was aged at 135 °C, reducing the time to failure compared to the lower thermal aging temperatures [44]. In contrast, when subjected to thermal aging at 115 °C for 1344 h, UHMWPE displayed a significant drop in molar mass, of around 70% [45]. This suggests that, when PP/UHMWPE-based samples are aged at 120 °C, the UHMWPE phase is more likely to break before the PP phase.

4.2. Fourier Transform Infrared Spectroscopy

The infrared spectral data obtained from unaged PP/UHMWPE blends and PP/UHMWPE/MgO nanocomposites are presented in Figure 6. The spectra include distinct bands corresponding to PP, UHMWPE, and overlapping bands from both the PP with UHMWPE phases, which aligns with the findings reported in the published literature [46,47]. In the PP/UHMWPE/MgO nanocomposite, a broad band below 700 cm^{-1} is attributed to the magnesium–oxygen bending vibration, as reported in previous studies [48,49].

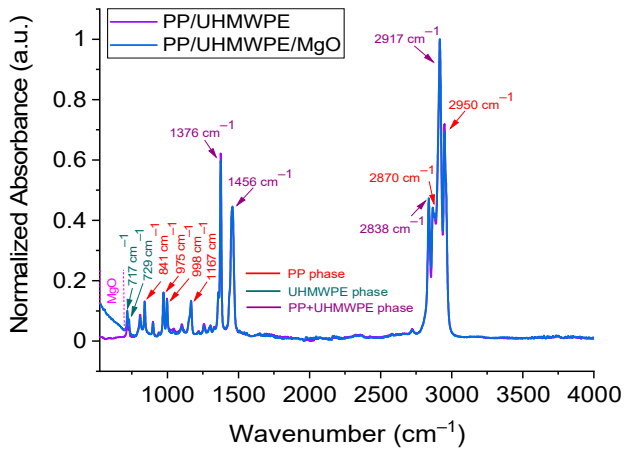

Figure 6. The FTIR spectrum of the unaged reference samples of PP/UHMWPE blend and PP/UHMWPE/MgO nanocomposite.

After undergoing thermal aging at 120 °C for a duration of 672 h, Figure 7 highlights the emergence of new infrared absorbance within the range of 1600–1900 cm^{-1}, corre-

sponding to carbonyl groups (C=O). The nanocomposites exhibit a lower peak intensity of carbonyl groups compared to the blends. Both the PP pellets and UHMWPE powder used to prepare the blends and nanocomposites were commercial materials and would be expected to contain antioxidants. The presence of antioxidants was observable in the FTIR spectra of some samples, but these signals, when detectable, were weak. Thus, it was not possible to make a precise identification, beyond suggesting that they appear to be related to phenolic-based antioxidants. Thereby, the variations in these carbonyl groups at different aging periods are likely to be linked to different oxidation reactions, a consequence of antioxidants and thermo-oxidative reactions [2,50].

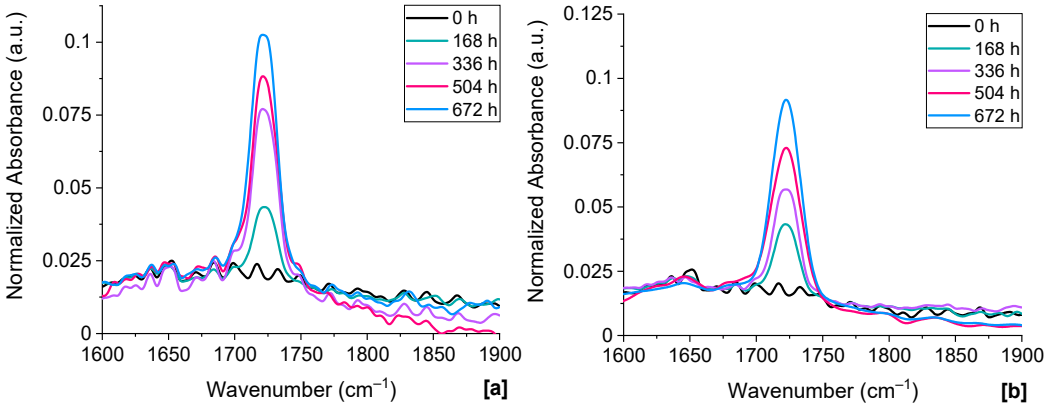

Figure 7. The FTIR absorption band of carbonyl groups under thermal aging in (**a**) PP/UHMWPE and (**b**) PP/UHMWPE/MgO.

The calculation of the CI, used to represent the degree of oxidation as illustrated in Figure 8, is based on the ratio of the peak areas of the carbonyl band (1600–1900 cm^{-1}) to the CH_2 scissoring band (1420 to 1500 cm^{-1}) [51]. Interestingly, the CI values of all tested samples do not exhibit a smooth trend with an increasing aging time. For aging durations below 336 h, the CI gradually increases, but beyond that point, it experiences a rapid rise, reaching a high value at 672 h. During the first 336 h, the oxidation process is inhibited by antioxidants within the system. As the aging periods further increase, the CI significantly increases, which is related to the consumption of antioxidants and a consequent acceleration of thermo-oxidative reactions [2].

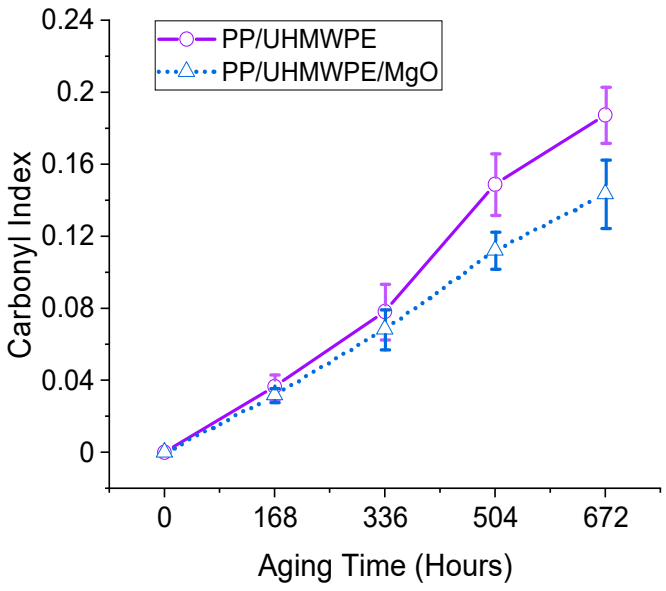

Figure 8. The calculated CI of PP/UHMWPE and PP/UHMWPE/MgO aged at 120 °C from 0 to 672 h.

4.3. Space Charge Dynamics

Figure 9 illustrates the space charge profiles obtained from PP/ UHMWPE and PP/UHMWPE/MgO after different aging periods at 120 °C. In the unaged samples, the nanocomposites exhibit lower charge injection from the cathode compared to the blends. This finding is consistent with previous studies when using a low filler content (<5 wt.%) of MgO in the polymer matrix [52,53]. After thermal aging, the PP/UHMWPE blends showed a gradual increase in the injection of homocharges from the cathode up to 336 h, after which, at 504 h, the homocharges significantly decreased, and charge injection was rarely observed. However, with further thermal aging up to 672 h in this blend, the injection of homocharges is once again significantly increased. On the other hand, for PP/UHMWPE/MgO, homocharges from the cathode are gradually injected into the samples, and in this system, a charge injection further increases up to 504 h before sharply decreasing at 672 h. This observed homocharge injection behavior is in line with the estimated total charge accumulation after 1 h of poling under +40 kV/mm (Figure 10), obtained by integration across the sample thickness using the subtraction method [54].

It appears that PP/UHMWPE/MgO nanocomposites display a lower charge accumulation than the unfilled blend counterparts. When considering this total charge together with the CI in Figure 8, both samples showed the lowest charge accumulation when the CI was around 0.15. This corresponds to 504 h aging in the unfilled system and 672 h aging in the MgO system. In short, MgO is slowing the aging (the rate of increase in CI), and this maps straight through to the space charge. It is therefore reasonable to conclude that the CI is a good indicator for space charge dynamics [21], as these carbonyl groups seem to act as (shallow) charge traps. The CI value of 0.15 appears to be a threshold value in the samples tested. Higher values of the index can be linked to significantly higher charge accumulation, as observed in the 672 h PP/UHMWPE blend.

Figure 11 presents normalized plots of the charge accumulation of PP/UHMWPE and PP/UHMWPE/MgO during the charge decay process over 3600 s. The results suggest that charge decay is faster after thermal aging in both samples. In the case of PP/UHMWPE, the decay rate is slower at 504 h before showing a significantly higher decay rate at 672 h. On the other hand, PP/UHMWPE/MgO exhibits a faster charge decay rate with an increasing aging time, only to slow down at 672 h of aging. When comparing PP/UHMWPE and PP/UHMWPE/MgO, the charge decay in the latter is slower, considering the equivalent aging conditions.

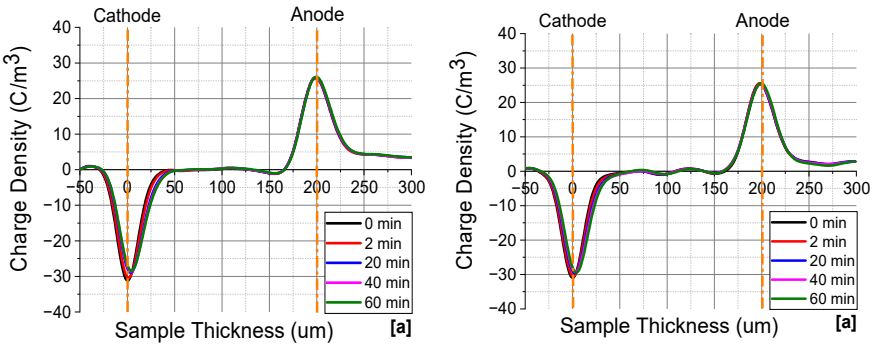

Figure 9. *Cont.*

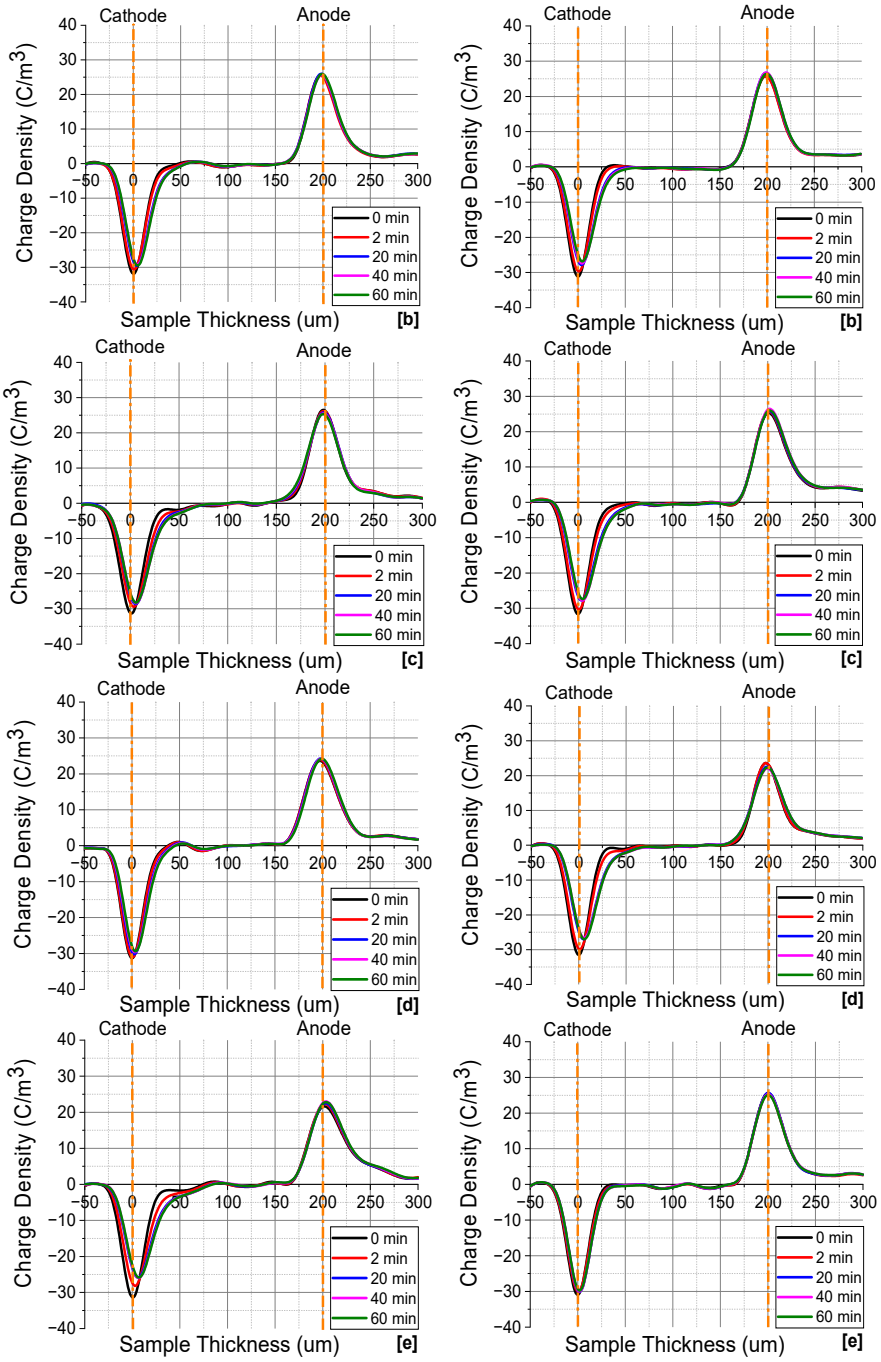

Figure 9. Space charge profile at the different aging times of 120 °C in PP/UHMWPE blends (**left**) and PP/UHMWPE/MgO nanocomposites (**right**) of (**a**) unaged, (**b**) 168 h, (**c**) 336 h, (**d**) 504 h, and (**e**) 672 h.

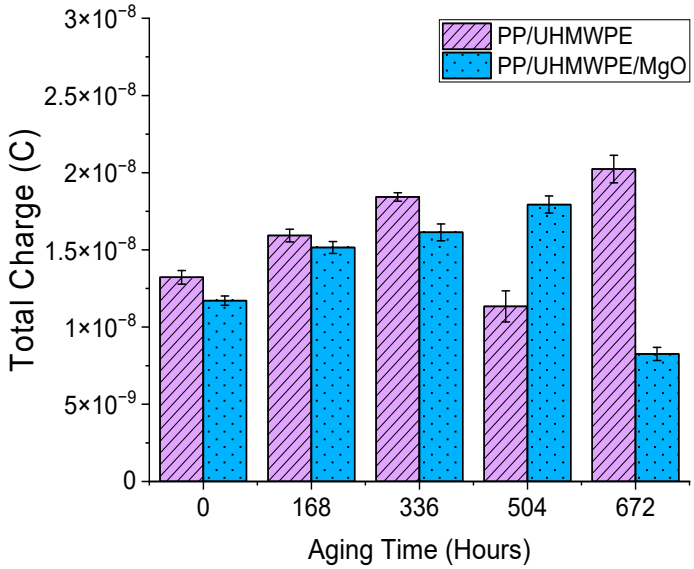

Figure 10. The total charge of thermally aged in PP/UHMWPE and PP/UHMWPE/MgO under +40 kV/mm.

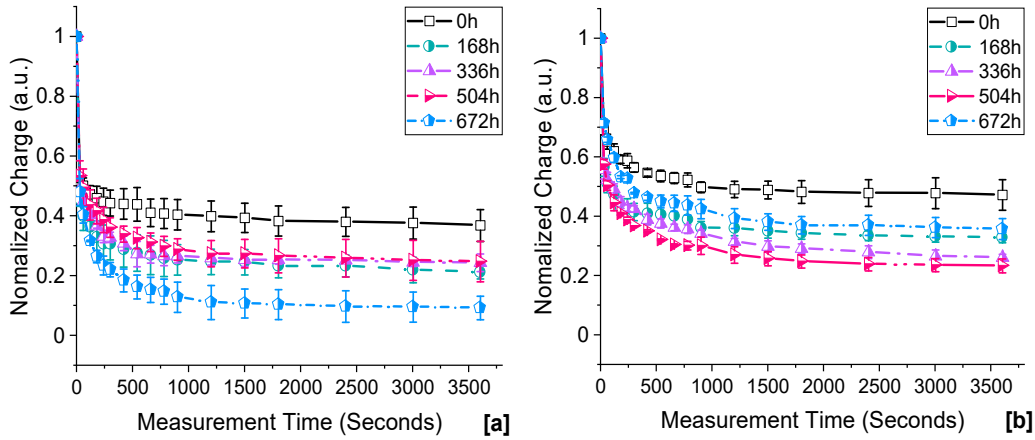

Figure 11. The normalized charge decay obtained from (**a**) PP/UHMWPE and (**b**) PP/UHMWPE/MgO aged from 0 to 672 h.

4.4. DC Conductivity

Figure 12 shows the time-dependent conductivity data obtained from PP/UHMWPE with and without MgO nanoparticles aged at 120 °C for periods up to 672 h. Due to the overlapping nature of the conductivity datasets, presenting all the data in the format shown in Figure 12 would lead to impaired clarity. Therefore, the impact of aging time on conductivity is represented using steady-state DC conductivity values, which were estimated by fitting the time-dependent data to the Curie–von Schweidler law [55].

From the results in Figure 13, it is evident that the magnitude of the conductivity exhibits non-monotonic behavior. For the unaged PP/UHMWPE and PP/UHMWPE/MgO samples, the derived conductivity reaches a steady-state at approximately 3.6×10^{-16} S/cm and 3.2×10^{-16} S/cm, respectively. These findings are consistent with the results in [13,56], which suggest that the addition of the low MgO filler content (<3 wt.%) results in somewhat lower conductivity compared to the unfilled samples.

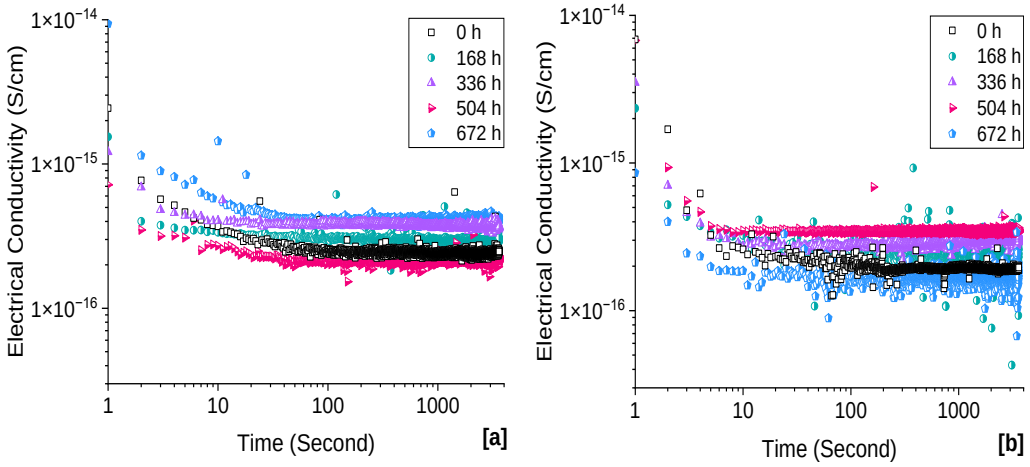

Figure 12. Time-dependent DC conductivity of (**a**) PP/UHMWPE and (**b**) PP/UHMWPE/MgO aged at 120 °C from 0 to 672 h.

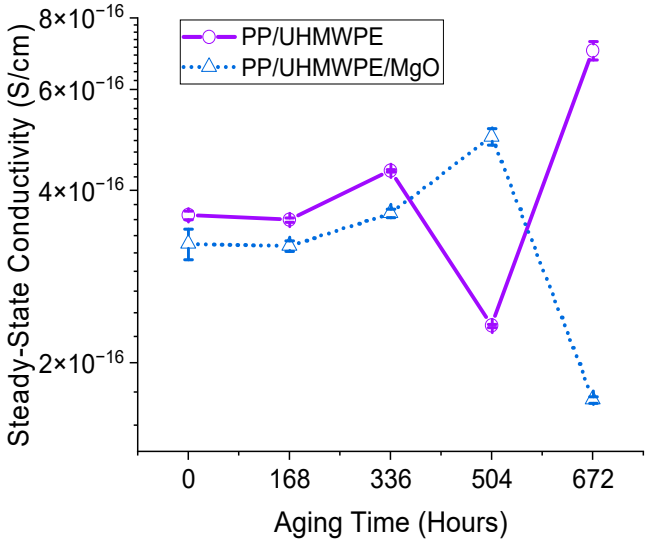

Figure 13. Steady-state DC conductivity of PP/UHMWPE and PP/UHMWPE/MgO aged from 0 to 672 h.

The effect of thermal aging initially led to a higher measured conductivity compared to the unaged samples. The behavior exhibited in Figure 13 is similar to the one described in the total charge amount shown in Figure 10. Once again, the reduced conductivity observed at 504 h for PP/UHMWPE and at 672 h for PP/UHMWPE/MgO is likely related to the critical carbonyl index of around 0.15.

5. Discussion

5.1. Aging, Structural Changes, and Chemical Characteristics

Thermo-oxidative aging in PP/UHMWPE and PP/UHMWPE/MgO follows a similar mechanism. During the 336-h aging period, the CI gradually increases with aging time. During this period, the oxidation process is inhibited by the antioxidant within the systems. Simultaneously, recrystallization, primarily observed in the UHMWPE phase, becomes dominant. This ongoing process results in an augmentation of the crystallinity and melting temperature of UHMWPE. Tantipattarakul et al. [21] demonstrated a similar phenomenon in aged LDPE/HDPE blends at 120 °C, where the T_m of the HDPE phase (124 °C) in the blends shifted to higher values with an increasing aging time. It is suggested that the increase in crystallinity and melting temperature is attributed to annealing effects, which are

enhanced by the initial stages of chain scission, facilitating lamellar recrystallization [57,58]. As the aging periods continue to increase, the CI experiences a significant increase. This stage is associated with the consumption of the antioxidant, as thermo-oxidative reactions occur rapidly. This reaction leads to chain scissions and decreases the thermal stability [59]. The diffusion of oxygen into the materials primarily occurs within the amorphous/melt phase [2,21,60]. This process subsequently inhibits recrystallization, leading to a reduction in crystallinity [2,21].

In comparison to PP/UHMWPE blends, nanocomposites demonstrate a lower occurrence of thermo-oxidative reactions, especially from 336 h onward, indicating their increased resistance to thermal aging. This observation is consistent with the findings in [11], where it was shown that the presence of MgO in XLPE delays thermo-oxidation reactions compared to unfilled XLPE. Additionally, results from [12,13] indicated that the use of MgO in LDPE effectively delayed thermo-oxidative reactions during aging, as opposed to composites filled with SiO_2, ZnO, or unfilled LDPE. The authors stated that the varied response of different nanocomposites to thermal aging can be attributed to their distinct thermal stability [13]. This phenomenon could be attributed to the interfacial interaction between nanoparticles and the polymer matrix, which hinders the breakage polymer chains during thermal aging. As a result, in the case of PP/UHMWPE, the absence of MgO makes the polymer more susceptible to chain scission, resulting in a more pronounced reduction in thermal stability [59].

Thermo-oxidative reactions occur throughout the interface regions between the two polymers, leading to the formation of more carbonyl groups. Unlike PP/UHMWPE blends, the inclusion of MgO nanoparticles as a compatibilizer in unaged samples [10,61] enhances the interfacial interaction between PP and UHMWPE. This results in reduced chain scission in nanocomposites, leading to better thermal stability [59]. As a consequence, the structural changes in nanocomposites are less pronounced during thermal aging, which hinders oxygen diffusion and leads to fewer carbonyl groups.

5.2. Aging and Charge Transport

The chemical and structural changes within PP/UHMWPE blends, as well as their nanocomposites, follow similar trends, with nanocomposites displaying slower changes compared to the blends. However, when considering charge accumulation and conductivity, these systems show different behaviors. Both systems exhibit an increase in charge accumulation and conductivity after thermal aging until a certain time. Beyond this specific period, the charge accumulation and conductivity significantly decrease compared to their unaged counterparts.

The lowest charge accumulation and conductivity are observed in both systems when the CI is around 0.15, which corresponds to 504 h of aging for PP/UHMWPE blends and 672 h of aging for PP/UHMWPE/MgO nanocomposites. This suggests that the addition of MgO to PP/UHMWPE blends results in slower aging, which corresponds to a reduced rate of CI increase, and this effect directly influences the charge accumulation and conductivity. These results align with the published literature [12,13], which demonstrates that LDPE/MgO nanocomposites delay thermo-oxidative reactions and effectively suppress charge accumulation compared to unfilled LDPE.

When the carbonyl index surpasses this critical threshold, both charge accumulation and conductivity significantly increase, leading to faster charge decay. Similar effects of thermal oxidation on the rate of charge decay have been previously reported [62,63], with the decay rate being linked to trap density and trap depth energy levels. Samples with lower concentrations of traps exhibit a slower decay of trapped charge, whereas an increase in the number of traps results in the faster decay of the trapped charge.

Carbonyl groups, consisting of C=O bonds, possess a different electronegativity compared to the hydrocarbon groups. When polar molecules with high electronegativity are introduced, the electronic structure at the interface is modified, effectively acting as traps within the interfaces and hindering the movement of charge carriers. This effect has been

observed in various studies [21,64,65], where the introduction of a low concentration of carbonyl groups into the systems reduces the effective charge carrier mobility.

6. Conclusions

In this work, the effects of thermo-oxidative aging in PP/UHMWPE and PP/UHMWPE/MgO were reported. PP/UHMWEP blends, as well as the respective MgO-nanocomposites, were aged at 120 °C up to 672 h. This shows that the thermo-oxidative aging of PP/UHMWPE and PP/UHMWPE/MgO follows a similar mechanism, with recrystallization dominating the initial 336 h of aging. This process leads to an increase in crystallinity and melting temperature. Beyond 336 h, the consumption of antioxidants promotes chain scission, leading to a decrease in crystallinity.

The presence of MgO nanoparticles as a compatibilizer in PP/UHMWPE blends delays the thermo-oxidative reactions and structural changes during thermal aging. This results in PP/UHMWPE/MgO having less charge accumulation and conductivity, implying a slower aging process compared to PP/UHMWPE blends. The carbonyl index plays a significant role in charge accumulation and conductivity behavior. The lowest charge accumulation when the carbonyl index is around 0.15, which aligns with 504 h of aging in the unfilled PP/UHMWPE system and 672 h of aging in the PP/UHMWPE/MgO system. Once the carbonyl index surpasses the critical threshold, both the charge accumulation and conductivity significantly increase.

Overall, this study provides details regarding the effects of thermo-oxidative aging behavior on changes in chemical, structure, and dielectric properties of PP/UHMWPE and PP/UHMWPE/MgO nanocomposites. The findings demonstrate the potential of these nanocomposites as insulation materials for HV insulation systems, highlighting the importance of considering thermal aging effects for long-term performance evaluation.

Author Contributions: Conceptualization, P.K., O.V., A.V. and T.A.; Methodology, P.K.; Validation, P.K., O.V., A.V. and T.A.; Formal analysis, P.K.; Investigation, P.K.; Writing—original draft, P.K.; Writing—review & editing, P.K., O.V., A.V. and T.A.; Supervision, A.V. and T.A. All authors have read and agreed to the published version of the manuscript.

Funding: This research was funded by the Royal Thai Government.

Data Availability Statement: Not applicable.

Conflicts of Interest: The authors declare no conflict of interest.

References

1. Kim, C.; Jin, Z.; Jiang, P.; Zhu, Z.; Wang, G. Investigation of dielectric behavior of thermally aged XLPE cable in the high-frequency range. *Polym. Test.* **2006**, *25*, 553–561. [CrossRef]
2. Li, H.; Li, J.; Ma, Y.; Yan, Q.; Ouyang, B. The role of thermo-oxidative aging at different temperatures on the crystal structure of crosslinked polyethylene. *J. Mater. Sci. Mater. Electron.* **2017**, *29*, 3696–3703. [CrossRef]
3. Liang, B.; Lan, R.; Zang, Q.; Liu, Z.; Tian, L.; Wang, Z.; Li, G. Influence of Thermal Aging on Dielectric Properties of High Voltage Cable Insulation Layer. *Coatings* **2023**, *13*, 527. [CrossRef]
4. Zhou, Y.; Dang, B.; Wang, H.; Liu, J.; Li, Q.; Hu, J.; He, J. Polypropylene-based ternary nanocomposites for recyclable high-voltage direct-current cable insulation. *Compos. Sci. Technol.* **2018**, *165*, 168–174. [CrossRef]
5. Rytoluoto, I.; Ritamaki, M.; Lahti, K.; Pasanen, S.; Pelto, J. Dielectric breakdown properties of mechanically recycled SiO_2-BOPP nanocomposites. *IEEE Int. Conf. Dielectr.* **2016**, *1*, 288–292. [CrossRef]
6. Maddah, H.A. Polypropylene as a Promising Plastic: A Review. *Am. J. Polym. Sci.* **2016**, *6*, 1–11.
7. Liu, W.; Cheng, L.; Li, S. Review of electrical properties for polypropylene based nanocomposite. *Compos. Commun.* **2018**, *10*, 221–225. [CrossRef]
8. Lindqvist, K.; Andersson, M.; Boss, A.; Oxfall, H. Thermal and Mechanical Properties of Blends Containing PP and Recycled XLPE Cable Waste. *J. Polym. Environ.* **2018**, *27*, 386–394. [CrossRef]
9. Patti, A.; Acierno, D. *Thermal Conductivity of Polypropylene-Based Materials*; IntechOpen: London, UK, 2020. [CrossRef]
10. Andritsch, T.; Ketsamee, P. Dielectric, thermal and mechanical properties of polypropylene/ultra—high molecular weight polyethylene nanocomposites for power cables. *CIGRE Int. Symp.* 2023; in press.
11. Paramane, A.; Chen, X.; Dai, C.; Guan, H.; Yu, L.; Tanaka, Y. Electrical insulation performance of cross-linked polyethylene/MgO nanocomposite material for ±320 kV high-voltage direct-current cable. *Polym. Compos.* **2019**, *41*, 1936–1949. [CrossRef]

12. Wang, Y.; Wang, C.; Zhang, Z.; Xiao, K. Anti-thermal aging properties of low-density polyethylene-based nanocomposites. *IEEE Trans. Dielectr. Electr. Insul.* **2018**, *25*, 1003–1013. [CrossRef]
13. Wang, Y.; Wang, C.; Zhang, Z.; Xiao, K. Effect of Nanoparticles on the Morphology, Thermal, and Electrical Properties of Low-Density Polyethylene after Thermal Aging. *Nanomaterials* **2017**, *7*, 320. [CrossRef]
14. Ke, K.; Wang, Y.; Liu, X.-Q.; Cao, J.; Luo, Y.; Yang, W.; Xie, B.-H.; Yang, M.-B. A comparison of melt and solution mixing on the dispersion of carbon nanotubes in a poly(vinylidene fluoride) matrix. *Compos. Part B Eng.* **2012**, *43*, 1425–1432. [CrossRef]
15. Passador, F.; Ruvolo-Filho, A.; Pessan, L. Nanocomposites of Polymer Matrices and Lamellar Clays. In *Nanostructures*; Elsevier Inc.: Amsterdam, The Netherlands, 2017; pp. 187–207. [CrossRef]
16. Drakopoulos, S.X.; Psarras, G.C.; Forte, G.; Martin-Fabiani, I.; Ronca, S. Entanglement dynamics in ultra-high molecular weight polyethylene as revealed by dielectric spectroscopy. *Polymer* **2018**, *150*, 35–43. [CrossRef]
17. Berenguer, J.P.; Berman, A.; Quill, T.; Zhou, T.; Kalaitzidou, K.; Cola, B.; Bougher, T.; Smith, M. Incorporation of polyethylene fillers in all-polymer high-thermal-conductivity composites. *Polym. Bull.* **2020**, *78*, 3835–3850. [CrossRef]
18. Guo, Y.; Cao, C.; Cheng, H.; Chen, Q.; Huang, B.; Luo, F.; Qian, Q. Thermal Performances of UHMWPE/BN Composites Obtained from Different Blending Methods. *Adv. Polym. Technol.* **2019**, *2019*, 8687450. [CrossRef]
19. Ketsamee, P.; Andritsch, T.; Vaughan, A. Effect of Surface-Modified TiO_2 and MgO Nanoparticles on Dielectric Permittivity and Breakdown Strength of PP Nanocomposites. In Proceedings of the 2021 IEEE Conference on Electrical Insulation and Dielectric Phenomena (CEIDP), Vancouver, BC, Canada, 12–15 December 2021; pp. 1–4. [CrossRef]
20. Ketsamee, P.; Andritsch, T.; Vaughan, A. The effects of humidity on dielectric permittivity of surface-modified TiO_2- and MgO-based polypropylene nanocomposites. *IEEE Trans. Dielectr. Electr. Insul.* **2023**, *30*, 82–89. [CrossRef]
21. Tantipattarakul, S.; Vaughan, A.S.; Andritsch, T. Ageing behaviour of a polyethylene blend: Influence of chemical defects and morphology on charge transport. *High Volt.* **2020**, *5*, 270–279. [CrossRef]
22. *IEC/TS 62758*; Calibration of Space Charge Measuring Equipment based on the Pulsed Electro-Acoustic (PEA) Measurement Principle. International Electrotechnical Commission: London, UK, 2012.
23. *ASTM D257-14*; Standard Test Methods for DC Resistance or Conductance of Insulating Materials. ASTM International: Conshohocken, PA, USA, 2021.
24. Azmi, A.; Lau, K.Y.; Ahmad, N.A.; Abdul-Malek, Z.; Tan, C.W.; Ching, K.Y.; Vaughan, A.S. Dielectric Properties of Thermally Aged Polypropylene Nanocomposites. *IEEE Trans. Dielectr. Electr. Insul.* **2022**, *29*, 543–550. [CrossRef]
25. Hu, S.; Wang, W.; Dang, B.; Zhou, Y.; Yuan, C.; Hu, J.; Li, Q.; He, J. Thermal properties and space charge behavior of thermally aged polypropylene/elastomer blends nanocomposite. *IEEE Trans. Dielectr. Electr. Insul.* **2020**, *27*, 521–527. [CrossRef]
26. Chiu, F.-C.; Chu, P.-H. Characterization of Solution-Mixed Polypropylene/Clay Nanocomposites without Compatibilizers. *J. Polym. Res.* **2005**, *13*, 73–78. [CrossRef]
27. Nishino, T.; Matsumoto, T.; Nakamae, K. Surface structure of isotactic polypropylene by X-ray diffraction. *Polym. Eng. Sci.* **2000**, *40*, 336–343. [CrossRef]
28. Unger, T.; Klocke, L.; Herrington, K.; Miethlinger, J. Investigation of the rheological and mechanical behavior of Polypropylene/ultra-high molecular weight polyethylene compounds related to new online process control. *Polym. Test.* **2020**, *86*, 106442. [CrossRef]
29. Kagenda, C.; Lee, J.W.; Memon, F.H.; Ahmed, F.; Samantasinghar, A.; Akhtar, M.W.; Khalique, A.; Choi, K.H. Silicone Elastomer Composites Fabricated with MgO and MgO-Multi-Wall Carbon Nanotubes with Improved Thermal Conductivity. *Nanomaterials* **2021**, *11*, 3418. [CrossRef]
30. Chen, Q.; Xiang, Z.; Yang, Q.; Kong, M.; Huang, Y.; Liao, X.; Niu, Y.; Zhao, Z. Flow-induced β-crystal of iPP in microinjection molding: Effects of addition of UHMWPE and the processing parameters. *J. Polym. Res.* **2016**, *23*, 16. [CrossRef]
31. Jin, M.; Jin, B.; Xu, X.; Li, X.; Wang, T.; Zhang, J. Effects of ultrahigh molecular weight polyethylene and mould temperature on morphological evolution of isotactic polypropylene at micro-injection moulding condition. *Polym. Test.* **2015**, *46*, 41–49. [CrossRef]
32. Sanaeepur, H.; Ahmadi, R.; Sinaei, M.; Kargari, A. Pebax-modified cellulose acetate membrane for CO_2/N_2 separation. *J. Membr. Sci. Res.* **2019**, *5*, 25–32.
33. Ding, M.; He, W.; Wang, J.; Wang, J. Performance evaluation of cross-linked polyethylene insulation of operating 110 kV power cables. *Polymers* **2022**, *14*, 2282. [CrossRef]
34. Wenig, W.; Fiedel, H.W.; Scholl, A. Crystallization kinetics of isotactic polypropylene blended with atactic polystyrene. *Colloid Polym. Sci.* **1990**, *268*, 528–535. [CrossRef]
35. Utracki, L.A.; Wilkie, C.A. Crystallization, micro- and nano-structure, and melting behavior of polymer blends. In *Polymer Blends Handbook*, 2nd ed.; Utracki, L.A., Wilkie, C.A., Eds.; Kluwer Academic Publishers: Dordrecht, The Netherlands, 2014; pp. 291–446.
36. Zhang, W.; Zou, L. Molecular Dynamics Simulations of Crystal Nucleation near Interfaces in Incompatible Polymer Blends. *Polymers* **2021**, *13*, 347. [CrossRef] [PubMed]
37. He, X.; Rytoluoto, I.; Anyszka, R.; Mahtabani, A.; Saarimaki, E.; Lahti, K.; Paajanen, M.; Dierkes, W.; Blume, A. Silica Surface-Modification for Tailoring the Charge Trapping Properties of PP/POE Based Dielectric Nanocomposites for HVDC Cable Application. *IEEE Access* **2020**, *8*, 87719–87734. [CrossRef]
38. Bond, E.B.; Spruiell, J.E.; Lin, J.S. A WAXD/SAXS/DSC study on the melting behavior of Ziegler-Natta and metallocene catalyzed isotactic polypropylene. *J. Polym. Sci. Part B Polym. Phys.* **1999**, *37*, 3050–3064. [CrossRef]

39. Lee, K.H.; Sinha, T.K.; Choi, K.W.; Oh, J.S. Ultra-high-molecular-weight polyethylene reinforced polypropylene and polyamide composites toward developing low-noise automobile interior. *J. Appl. Polym. Sci.* **2019**, *137*, 48720. [CrossRef]
40. Krache, R.; Benavente, R.; López-Majada, J.M.; Pereña, J.M.; Cerrada, M.L.; Pérez, E. Competition between α, β, and γ polymorphs in a β-nucleated metallocenic isotactic polypropylene. *Macromolecules* **2007**, *40*, 6871–6878. [CrossRef]
41. Boukezzi, L.; Boubakeur, A.; Lallouani, M. Effect of artificial thermal aging on the crystallinity of XLPE insulation cables: X-ray study. In Proceedings of the 2007 Annual Report-Conference on Electrical Insulation and Dielectric Phenomena, Vancouver, BC, Canada, 14–17 October 2007; pp. 65–68. [CrossRef]
42. Zhang, L.; Wu, W.; Teng, C.; Meng, S. Mechanical properties and space charge behavior of thermally aged polypropylene/elastomer blends. *J. Electrost.* **2022**, *115*, 103673. [CrossRef]
43. Azmi, A.; Lau, K.Y.; Ahmad, N.A.; Abdul-Malek, Z.; Tan, C.W.; Ayop, R. Thermal and Dielectric Properties of Thermally Aged Polypropylene/Calcium Carbonate Nanocomposites. In Proceedings of the 2020 IEEE International Conference on Power and Energy (PECon), Penang, Malaysia, 7–8 December 2020; pp. 255–258. [CrossRef]
44. Grabmann, M.K.; Wallner, G.M.; Maringer, L.; Buchberger, W.; Nitsche, D. Hot air aging behavior of polypropylene random copolymers. *J. Appl. Polym. Sci.* **2018**, *136*, 47350. [CrossRef]
45. Tsinas, Z.; Orski, S.V.; Bentley, V.R.C.; Lopez, L.G.; Al-Sheikhly, M.; Forster, A.L. Effects of Thermal Aging on Molar Mass of Ultra-High Molar Mass Polyethylene Fibers. *Polymers* **2022**, *14*, 1324. [CrossRef] [PubMed]
46. Liu, G.; Chen, Y.; Li, H. Study on processing of ultrahigh molecular weight polyethylene/polypropylene blends. *J. Appl. Polym. Sci.* **2004**, *94*, 977–985. [CrossRef]
47. Sutar, H.; Sahoo, P.C.; Sahu, P.S.; Sahoo, S.; Murmu, R.; Swain, S.; Mishra, S.C. Mechanical, Thermal and Crystallization Properties of Polypropylene (PP) Reinforced Composites with High Density Polyethylene (HDPE) as Matrix. *Mater. Sci. Appl.* **2018**, *9*, 502–515. [CrossRef]
48. Kandiban, M.; Vigneshwaran, P.; Potheher, V.I. Synthesis and characterization of MgO nanoparticles for photocatalytic applications. In Proceedings of the National Conference on Advances in Crystal Growth and Nanotechnology, Biddeford, ME, USA, 21 October 2015; pp. 1–5.
49. Salman, K.D.; Abbas, H.H.; Aljawad, H.A. Synthesis and characterization of MgO nanoparticle via microwave and sol-gel methods. *J. Phys. Conf. Ser.* **2021**, *1973*, 012104. [CrossRef]
50. Shibryaeva, L. *Thermal Oxidation of Polypropylene and Modified Polypropylene-Structure Effects*; IntechOpen: London, UK, 2012; pp. 63–86.
51. Almond, J.; Sugumaar, P.; Wenzel, M.N.; Hill, G.; Wallis, C. Determination of the carbonyl index of polyethylene and polypropylene using specified area under band methodology with ATR-FTIR spectroscopy. *e-Polymers* **2020**, *20*, 369–381. [CrossRef]
52. Zhou, Y.; Hu, J.; Dang, B.; He, J. Effect of different nanoparticles on tuning electrical properties of polypropylene nanocomposites. *IEEE Trans. Dielectr. Electr. Insul.* **2017**, *24*, 1380–1389. [CrossRef]
53. Zha, J.-W.; Wang, Y.; Wang, S.-J.; Zheng, M.-S.; Bian, X.; Dang, Z.-M. Space charge suppression in environment-friendly PP nanocomposites by employing freeze-dried MgO with foam nanostructure for high-voltage power cable insulation. *Appl. Phys. Lett.* **2019**, *114*, 252902. [CrossRef]
54. Liu, N.; Zhou, C.; Chen, G.; Zhong, L. Determination of threshold electric field for charge injection in polymeric materials. *Appl. Phys. Lett.* **2015**, *106*, 192901. [CrossRef]
55. Guot, T.C.; Guoi, W.W. A transient-state theory of dielectric relaxation and the Curie-von Schweidler law. *J. Phys. C Solid State Phys.* **1983**, *16*, 1955.
56. Pallon, L.K.H.; Hoang, A.T.; Pourrahimi, A.M.; Hedenqvist, M.S.; Nilsson, F.; Gubanski, S.; Gedde, U.W.; Olsson, R.T. The impact of MgO nanoparticle interface in ultra-insulating polyethylene nanocomposites for high voltage DC cables. *J. Mater. Chem. A* **2016**, *4*, 8590–8601. [CrossRef]
57. Khabbaz, F.; Albertsson, A.-C.; Karlsson, S. Chemical and morphological changes of environmentally degradable polyethylene films exposed to thermo-oxidation. *Polym. Degrad. Stab.* **1999**, *63*, 127–138. [CrossRef]
58. Anandakumaran, K.; Stonkus, D.J. Assessment of oxidative thermal degradation of crosslinked polyethylene and ethylene propylene rubber cable insulation. *Polym. Eng. Sci.* **1992**, *32*, 1386–1393. [CrossRef]
59. Ketsamee, P.; Saeedi, I.; Vaughan, A.; Andritsch, T. Dielectric permittivity and breakdown strength of thermally aged polypropylene/ultra–high molecular weight polyethylene nanocomposites. In Proceedings of the IEEE Conference on Electrical Insulation and Dielectric Phenomena, East Rutherford, NJ, USA, 15–19 October 2023.
60. Liu, J.; Wang, Y.; Xiao, K.; Zhang, Z. Research on the Thermal Aging Behaviors of LDPE/TiO_2 Nanocomposites. *J. Nanomater.* **2017**, *2017*, 5048382. [CrossRef]
61. Ketsamee, P.; Andritsch, T.; Vaughan, A. An Investigation of Mechanical Properties and Breakdown Strength of Polypropylene/Ultra-High Molecular Weight Polyethylene Nanocomposites. In Proceedings of the 2022 IEEE Conference on Electrical Insulation and Dielectric Phenomena (CEIDP), Denver, CO, USA, 2 November 2022; pp. 475–478. [CrossRef]
62. Men, R.; Lei, Z.; Song, J.; Li, Y.; Lin, L.; Tian, M.; Fabiani, D.; Xu, X. Effect of thermal ageing on space charge in ethylene propylene rubber at DC voltage. *IEEE Trans. Dielectr. Electr. Insul.* **2019**, *26*, 792–800. [CrossRef]
63. Ouyang, B.; Li, H.; Zhang, X.; Wang, S.; Li, J. The role of micro-structure changes on space charge distribution of XLPE during thermo-oxidative ageing. *IEEE Trans. Dielectr. Electr. Insul.* **2017**, *24*, 3849–3859. [CrossRef]

64. Tantipattarakul, S.; Vaughan, A.S.; Andritsch, T. On the influence of chemical defects and structural factors on charge transport and failure in polyethylene. *IEEE Trans. Dielectr. Electr. Insul.* **2020**, *27*, 288–295. [CrossRef]
65. Karlsson, M.E.; Xu, X.; Hillborg, H.; Ström, V.; Hedenqvist, M.S.; Nilsson, F.; Olsson, R.T. Lamellae-controlled electrical properties of polyethylene-morphology, oxidation and effects of antioxidant on the DC conductivity. *RSC Adv.* **2020**, *10*, 4698–4709. [CrossRef] [PubMed]